Desalination and Water Treatment
www.deswater.com

doi: 10.5004/dwt.2020.25970

201 (2020) 338–348
October

Efficiency and mechanism of phenacetin decomposition in Al_2O_3 supported Ni–Co layered double hydroxides catalytic ozonation

Tingting Zhan, Siqi Fan, Pan Xiong, Xinze Bian, Yi Xia, Lin Wang, Wan Zhou, Qizhou Dai*, Jianmeng Chen

College of Environment, Zhejiang University of Technology, Hangzhou 310032, China, Tel. +86 571 88320276; Fax: +86 571 88320276; email: dqz@zjut.edu.cn (Q. Dai)

Received 3 December 2019; Accepted 11 April 2020

ABSTRACT

In this research, Ni/Co/Fe 2D nanosheets-crosslinked frameworks (Ni–Co LDHs, Ni–Fe LDHs, Co–Fe LDHs) were synthetized to achieve a better performance on phenacetin (PNT) degradation in catalytic ozonation. The mechanism of enhanced degradation efficiency and mineralization in catalytic ozonation system were explored with the help of different kinds of catalysts characterization, including X-ray diffraction, Fourier transform infrared, Brunauer–Emmett–Teller, scanning electron microscopy, and energy-dispersive X-ray. The results showed that Ni–Co LDHs@Al_2O_3 catalyst could not only greatly enhance the degradation of PNT, but also have better stability and reusability by ozonation. The COD removal with Ni–Co LDHs@Al_2O_3 catalyst could reach 65.3%, while 63.8% with Ni–Co layered double hydroxides (LDHs) catalyst, 61.8% with Fe–Co LDHs catalyst, 55.5% with Ni–Fe LDHs catalyst and only 48% with ozonation alone after 120 min. In addition, based on the intermediates detected by gas chromatography-mass spectrometry, a possible degradation pathway of PNT was proposed.

Keywords: Catalytic ozonation; Ni–Co LDHs@Al_2O_3; Phenacetin; Degradation pathways

1. Introduction

Pharmaceuticals have received growing attention as new types of emerging contaminants (ECs) in surface [1] and ground waters [2] due to their extensive use and the difficulty in metabolic degradation. Several studies showed that they are not degraded effectively by traditional wastewater treatment processes [3,4]. And they have been observed that a potential risk to human health and ecological safety for the presence of pharmaceuticals in water [5]. As a pain-relieving and fever-reducing drug, phenacetin (PNT, N-(4-ethoxyphenyl) acetamide) was banned in US from 1983 for the side effect and after-effect of carcinogenesis [6]. Until now, it is still widely used in some Asian countries and the concentration of PNT pharmaceutical was increased in China's wastewater treatment plant [7]. If PNT pharmaceutical could be efficiently removed in the discharge of the pharmaceutical enterprise wastewater, it would greatly reduce the pollution and concentration level in water environment. In recent, several water industry technologies were used to remove PNT from water, such as ozonation, UV photolysis [8], photocatalytic degradation [9], Fenton reaction [10], and combinations of these techniques [11]. Zhu et al. [8] reported that the degradation of PNT by the combination of low-pressure mercury lamp and chlorine (UV/ chlorine), was systematically investigated in terms of degradation kinetics. The degradation of PNT followed pseudo-first-order kinetics. Qi et al. [7] reported that the magnetic spinel $CuFe_2O_4$ (CFO) had an excellent degradation of PNT in catalytic ozonation.

* Corresponding author.

Ozone (O_3) is known as a powerful oxidant in the aqueous medium which reacts either by ozone direct electrophilic attack or hydroxyl (•OH) radical indirect reaction [12]. However, it does not provide complete mineralization in many cases (monitored by chemical oxygen demand (COD)) [13]. Catalytic ozonation has gained more interest in order to provide better degradation efficiency. A wide variety of solid catalysts have been investigated so far, including metal transition metal based materials (single or supported metal oxide/oxyhydroxide) [14,15], zeolites [16,17], clay minerals [17], and activated carbon [18].

Among these catalysts, layered double hydroxides (LDH) are also termed hydrotalcite-like compounds or anionic clays, $[M^{2+}_{1-x}M^{3+}_{x}(OH)_2]\cdot[A_{x/n}]^{n-}\cdot mH_2O$, where M^{2+} is a divalent metal cation, M^{3+} is a trivalent metal cation, and A^{n-} is the exchangeable charge compensating anions [19]. These nanomaterials have been widely used in electrocatalytic reactions [20], photodegradation [21] and catalytic ozonation [13], due to the wide choice of transition metals and the abundance of hydroxyl groups in the layer structure. In recent years, El Hassani et al. [13] studied the catalytic activity of Ni-based layered double hydroxides (Ni-LDHs) nanomaterials for dye degradation (methyl orange (MO)) where the mineralization of MO increased in the presence of the catalyst compared to noncatalytic degradation. Xu et al. [22] used Co–Fe LDHs to support the formation of •OH by promoting ozone decomposition, and the degradation of ATL and TOC was significantly improved during the catalytic ozonation. This was due to the presence of different transition metals in LDH that enhanced ozone decomposition to form •OH radicals or other reactive species. Inspired by these results, we assumed that the Ni–Co LDHs/Ni–Fe LDHs/Co–Fe LDHs might have similar catalysis in ozonation for organic matter removal. However, the way to effectively immobilize or separate the LDHs particles is still a challenge in this catalytic ozonation system. Supported nanoparticle catalysts offer a promising approach to solve this problem. Among them, Al_2O_3 has been chosen because of its remarkable specific surface area and high stability [23]. Since LDHs covered on the surface of Al_2O_3, enhanced a better dispersion of nanoparticles in suspension [24], satisfied results can be reached at a certain condition. In addition, few studies on this kind of LDHs@Al_2O_3 catalyst and catalytic ozonation of pharmaceutical wastewater by this kind of catalyst have been reported.

In this study, Ni–Co LDHs/Ni–Fe LDHs/Co–Fe LDHs were prepared by the precipitation method and the catalytic activity of as-prepared samples were evaluated in the catalytic ozonation of PNT. The characterization techniques used to probe these catalysts were X-ray diffraction (XRD), Fourier transform infrared (FT-IR), scanning electron microscopy (SEM), and energy-dispersive X-ray (EDX). The recovery, stability and the metal leaching of the Ni–Co LDHs and Ni–Co LDHs@Al_2O_3 were compared, and the effect of the pH, initial PNT concentration, ozone dosage on the decomposition kinetics of PNT and COD were investigated and deeply analyzed. Finally, the organic and inorganic intermediates of PNT were identified by gas chromatography–mass spectrometry (GC/MS) and ion chromatography (IC), respectively, and possible degradation pathway of PNT and the reaction mechanism of ozonation catalyzed by Ni–Co LDHs@Al_2O_3 catalyst were proposed.

2. Experimental

2.1. Materials and reagents

PNT and all the other reagents were purchased from Aladin Chemical Company of China. Acetonitrile was of chromatographic reagent grade and other chemicals used in the experiments were of analytical reagent grade if not otherwise noted. Throughout this study, the initial pH of the solutions was adjusted to 9.0 by NaOH or H_2SO_4 solution. All the solutions were prepared with deionized water, and the initial concentration of simulative wastewater was 200 mg L^{-1}.

Synthesis of Ni–Co LDHs@Al_2O_3 nanoparticles: Ni–Co LDHs were supported on γ-Al_2O_3 by co-precipitation method with continuous nitrogen gas bubbling. γ-Al_2O_3 carriers had a diameter of 1–3 mm, a surface area of 450 m^2 g^{-1}. In a typical procedure, 2 g γ-Al_2O_3 was added to the solution, which containing 0.5 M of $Co(NO_3)_3\cdot 6H_2O$ and 0.5 M of $Ni(NO_3)_2\cdot 6H_2O$. After the pH was adjusted slowly to 9.0 using 1.0 M sodium hydroxide solution under vigorously magnetic stirring, the resulting suspension was transferred immediately into Teflon tubes and kept at 383 K for 19 h. The sample was grounded and sieved out using screen mesh (100 mesh) for further use. For a reference, Ni–Co LDHs were also prepared by repeating the same procedure described above except the addition of mesoporous γ-Al_2O_3. In addition, Co–Fe LDHs and Ni–Fe LDHs were synthesized using the same method, respectively. The characterization of the catalyst was shown in Fig. 2.

2.2. Catalytic ozonation procedure

Fig. 1 shows the schematic diagram of the catalytic ozonation system. The experimental apparatus employed in this work consisted of a cylindrical Pyrex glass reactor (an internal circulation reactor; volume 1.5 L), which solves the problem that the ozone utilization rate of the conventional equipment is low and the catalyst distribution is uneven. The reactor is operated at room temperature, ozone was produced from pure oxygen by an ozone generator (CFY-3, Hangzhou Rongxin Ltd.), which was bubbled into the bottom of the reactor. And the catalyst Co–Ni LDHs@Al_2O_3 forms an internal circulation-type gas–solid–liquid three-phase fluidized bed in the system. Ozone oxidation experiments were carried out by changing parameters such as ozone dosage (control gas source flow), simulated wastewater concentration of PNT and pH. The samples were taken from the top of the reactor at predetermined time points and filtered through a 0.22 μm pore size membrane filter for analysis. Excess ozone exhaust enters the potassium iodide absorption bottle. Same conditions were used for the sole ozonation process (without catalyst) and PNT adsorption on the catalyst (purging oxygen only without ozone). After the tests, the used catalysts were recovered from the mixture by standing precipitation separation, washed, and dried for use in subsequent tests.

2.3. Analytical methods

The concentration of PNT was analyzed using a high-performance liquid chromatography (HPLC, Model e2695,

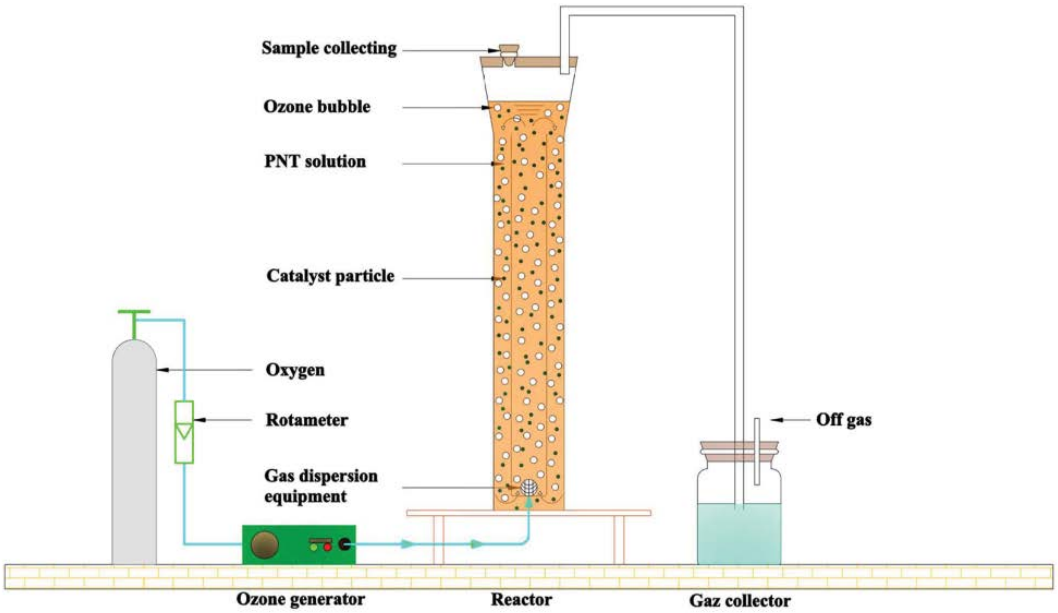

Fig. 1. Experimental equipment.

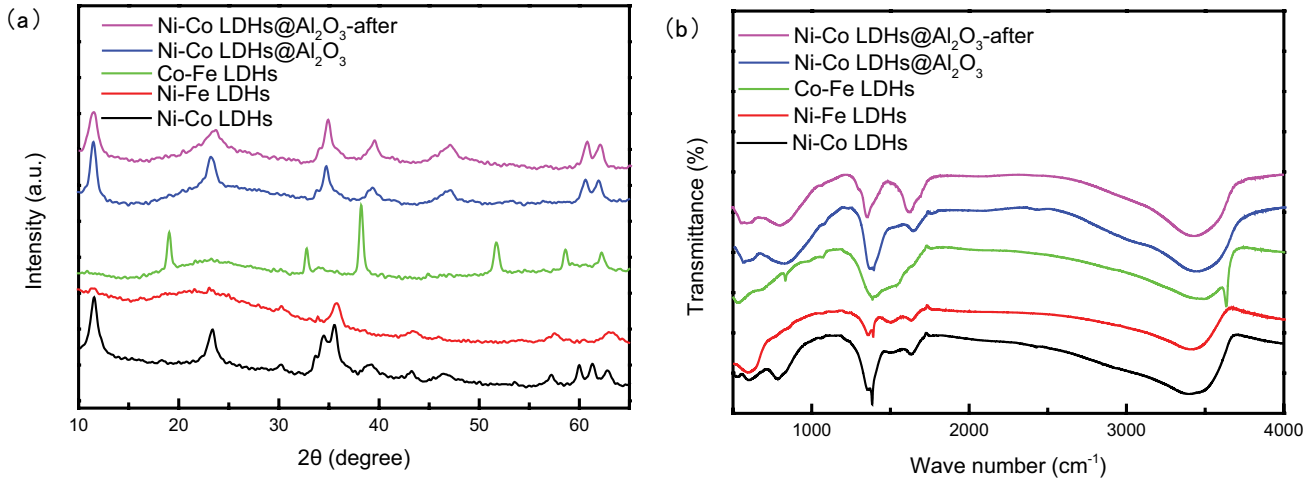

Fig. 2. (a) X-ray diffractograms of Ni–Fe LDHs, Fe–Co LDHs, Ni–Co LDHs, Ni–Co LDHs@Al_2O_3, Ni–Co LDHs@Al_2O_3-after and (b) FI-TR spectra of Ni–Fe LDHs, Fe–Co LDHs, Ni–Co LDHs, Ni–Co LDHs@Al_2O_3, Ni–Co LDHs@Al_2O_3-after.

Waters Technologies, USA) equipped with a C18 reversed phase column (XBridge, Waters Technologies, USA). The mobile phase was 75% CH_3CN and 25% phosphoric acid solution (0.08%). The flow rate was set at 1 L min^{-1} with the column temperature at 30°C. Injection volume was 10 μL, and the UV detector wavelength was set at 210 nm. Also, the COD value was determined using the standard method [25]. The indigo method or iodometric method was used to monitor the dissolved or gas ozone concentration, respectively. The pH value of the solutions was detected by a pH meter (LeiCi pHs-3E, Shanghai Jingke Co., Ltd., China). The identification of intermediates was conducted by a Thermo Quest Finnigan LCQ Duo mass spectrometer system (ion trap mass spectrometer) which was equipped with an electrospray ionization interface operating at electrospray ionization mode (LC-ESI/MS). ESI/MS data were acquired over a scan range between 50 and 1,000 Da. The mobile phase (0.8 mL/min) was delivered by a gradient system from a Thermo P4000.The mobile phase was a mixture of 0.1% formic acid (A) and acetonitrile solution containing 0.1% formic acid (B), which was carried out according to the following gradient mode: (1) 95% of A was kept during the first 3 min; (2) from 3 to 10 min, B was linearly increased from 5% to 50%, while A was steadily decreased to 50%, then held for 10 min; (3) from 25 to 50 min, the mobile phase was returned to the initial composition until the end of the run. The leached ions were measured by acidification digestion pretreatment and inductively coupled plasma-atomic emission spectrometry (ICP-AES) (PerkinElmer, USA) analysis method.

3. Results and discussion

3.1. Catalyst characterization

The formation of hydrotalcite phase was favored by a M^{2+}:M^{3+} molar ratio with the range of 1–5:1, which is M^{2+}:M^{3+} ratio within the range of 1:1 in this study. It has been reported that the LDHs surface area affected with the M^{2+}:M^{3+} ratios [26]. However, few studies on exploring the better catalytic activity of Ni–Fe LDHs, Fe–Co LDHs, and Ni–Co LDHs, and catalytic ozonation of pharmaceutical wastewater by this kind of catalyst have been reported.

3.1.1. XRD, FT-IR, and BET analysis of the samples

XRD is an effective method for identifying the phases present in the prepared catalysts [27]. The XRD patterns in Fig. 2a shows that the pristine Ni–Fe LDHs, Fe–Co LDHs, and Ni–Co LDHs with different bimetals were in good consistent with the standard patterns for the α-$Ni(OH)_2$ (JCPDS 38-0715), FeOOH (JCPDS 29-713), β-$Co(OH)_2$ (JCPDS 30-443), and Ni–Co LDH (JCPDS no. 38-0715), respectively, and no peaks from other crystal phases were detected. Such as the diffraction peaks of Ni–Co LDHs at 2θ = 11.8°, 23.3°, 35.3°, 39.6°, and 62.6°with the indices of (003), (006), (009), (015), and (110) displayed the characteristic reflections corresponding to hydrotalcite-like materials [28,29]. In addition, the pattern of Ni–Co LDHs@Al_2O_3 hybrid contains the diffraction peaks of both Ni–Co LDHs and γ-Al_2O_3, indicating the successfully supported of Ni–Co LDH on the γ-Al_2O_3, and the covering of Ni–Co LDH nanoflakes results in weakened peaks for γ-Al_2O_3. Among all the LDHs, Ni–Co LDHs@Al_2O_3 exhibited the best crystalline phase, it was not hard to learn that Ni–Co LDHs@Al_2O_3 had a structure of high stability, since the XRD pattern of Ni–Co LDHs@Al_2O_3 had almost no shift after participating in ozonation.

FT-IR is an appropriate technique to study chemical adsorption or chemical interaction [27]. The results obtained were similar for all the LDHs, and their profiles are shown in Fig. 2b. The FT-IR spectra of the LDHs between 500 and 4,000 cm^{-1} was shown in Fig. 2b. The band at 520 cm^{-1} was a fingerprint of O–Metal–O stretching, the band observed at 1,360 cm^{-1} was from the stretching of CO_3^{2-} ions in the interlayers, and the weak band of near 1,640 cm^{-1} could be interpreted as the H–O–H stretching modes and bending vibration of the free or adsorbed water [30]. The broad-band around 3,500–3,600 cm^{-1} was assigned to Metal–OH stretching [31]. Ni–Co LDHs@Al_2O_3 after ozonation clearly showed no difference compared to fresh catalyst. Noting, two peaks changed slightly at 1,360 and 1,640 cm^{-1} which carbonate loss and H–O–H increased after the reaction. We could also explain that due to the scavenging effect of CO_3^{2-}, it would react with $^{\bullet}OH$ during the reaction and further affect the degradation of organic pollutants. This result confirmed the existence of indirect reactions during catalytic ozonation degradation and the role of catalyst surface in enhancing the activation/decomposition of ozone molecules.

Furthermore, the surface area, pore volume, and average pore diameter of the as-prepared Ni–Fe LDHs, Fe–Co LDHs, Ni–Co LDHs, Ni–Co LDHs@Al_2O_3 before and after degradation of PNT were assessed by Brunauer–Emmett–Teller (BET) characterization, as shown in Table 1. The BET surface area value of the Ni–Co LDHs was estimated to be 184.8 $m^2\ g^{-1}$, which was larger than that of Ni–Fe LDHs (102.2 $m^2\ g^{-1}$) and Fe–Co LDHs (138.6 $m^2\ g^{-1}$). The result shows that the 2D layered nanosheet structure of Ni–Co was more stable and had a larger specific surface area, which matches the previous XRD. And the adsorption characteristic changed similar to the variation of BET surface area [32]. Additionally, we found that growing the Ni–Co LDHs on the Al_2O_3 increased specific surface area and pore volume, promoted the catalytic activity of the catalyst [33]. The BET surface area and pore volume of the obtained Ni–Co LDHs@Al_2O_3 was 360.1 $m^2\ g^{-1}$ and 0.35 $cm^3\ g^{-1}$, and the average pore size was 14.63 nm, respectively. However, the surface area and pore diameter of the catalyst are reduced after the ozone reaction, it can be attributed to the destruction of the surface layer structure during the reaction, which corresponds to the increase in pore volume.

3.1.2. SEM and EDX studies of the samples

In this work, we found that as-produced Ni–Co LDHs@Al_2O_3 have the 2D nanosheets-crosslinked network structure we designed as shown in Figs. $3a_1$ and b_1, while the Ni–Co LDHs has the 2D particulate nanosheet-layered structure. All the samples showed a layered morphology and aggregated together forming micro-grade particles due to the existence of water [34]. The SEM images in Fig. 3a show that the Ni–Co LDHs is built from the excessively aggregated nanosheets, while the Fig. $3b_2$ indicates that Ni–Co LDHs@Al_2O_3 consists of outstretched and orderly nanosheets. It could be inferred from these observation results that γ-Al_2O_3 have considerable influence on the microscopic morphology of frameworks [35]. It is reasonable to believe that the Ni–Co LDHs@Al_2O_3 nanosheets have sufficient strength to keep outstretched state [36]. The SEM

Table 1
Results of BET characterization

	S_{BET} ($m^2\ g^{-1}$)	Average pore diameter (nm)	pore volume ($cm^3\ g^{-1}$)
Ni–Fe LDHs	102.25	9.18	0.23
Fe–Co LDHs	138.64	7.03	0.24
Ni–Co LDHs	184.80	6.23	0.28
Ni–Co LDHs@Al_2O_3	360.15	14.62	0.35
Ni–Co LDHs@Al_2O_3-after	330.38	12.71	0.37

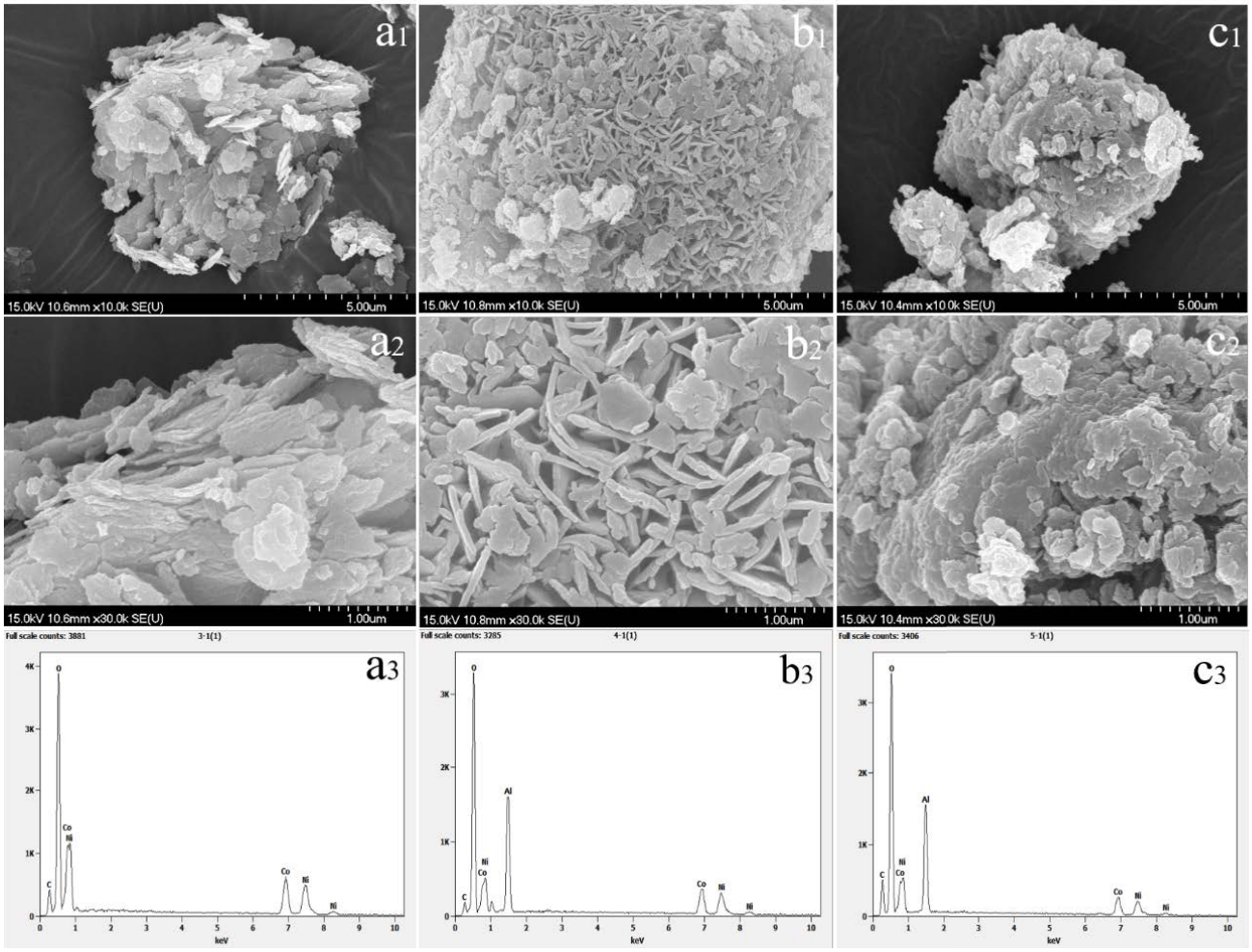

Fig. 3. SEM micrographs obtained from (a_1–a_3) Ni–Co LDHs, (b_1–b_3) Ni–Co LDHs@Al_2O_3, and (c_1–c_3) Ni–Co LDHs@Al_2O_3-after.

(Figs. 3b and c) and EDX analyses of the Ni–Co LDHs@Al_2O_3 were carried before and after ozonation. The profile of Ni–Co LDHs after ozonation was slightly different from the original without clear apparent structure, indicating an influence of ozonation on its hydroxide layer composition [37]. In addition, the EDX results (Table 2 and Figs. 3a_3–c_3) reveals the co-existence of Ni, Co, and Al elements in Ni–Co LDHs@Al_2O_3 with the atom percentage of 30.08%, 28.67%, and 41.25%, in agreement with the experimental molar ratio. The content of Ni–Co in Ni–Co LDHs@Al_2O_3 decreased after catalytic ozonation, which possibly due to partial metal leaching caused by the destruction of its structure in the ozone environment, and can be verified by ICP.

Table 2
Textural property of virgin and reacted samples

	Element Line	Weight %	Atom %
Ni–Co LDHs	Co K	49.36	49.27
	Ni K	50.64	50.73
Ni–Co LDHs@Al_2O_3	Al K	24.36	41.25
	Co K	36.99	28.67
	Ni K	38.65	30.08
Ni–Co LDHs@Al_2O_3-after	Al K	29.82	48.09
	Co K	34.41	25.40
	Ni K	35.77	26.51

3.2. Catalytic activity measurements for ozonation of PNT

As shown in Fig. 4, the catalytic activity of as-prepared catalysts (Ni–Fe LDHs, Fe–Co LDHs, and Ni–Co LDHs) was evaluated by the degradation and mineralization of PNT. The adsorption of PNT by catalyst was negligible during the reaction period with 4% of PNT removal rate by various LDHs during the control experiment with 12 mg min^{-1} oxygen dosage. However, rapid degradation of PNT was achieved in Ni–Fe LDHs, Fe–Co LDHs, and Ni–Co LDHs processes with initial parameters of 20°C, pH 9, 2 g L^{-1} catalyst, 12 mg min^{-1} ozone dosage and 200 mg L^{-1} initial concentration, indicating the high catalytic ability of Ni–Fe LDHs, Fe–Co LDHs, and Ni–Co LDHs. All groups of PNT obtained near complete removal

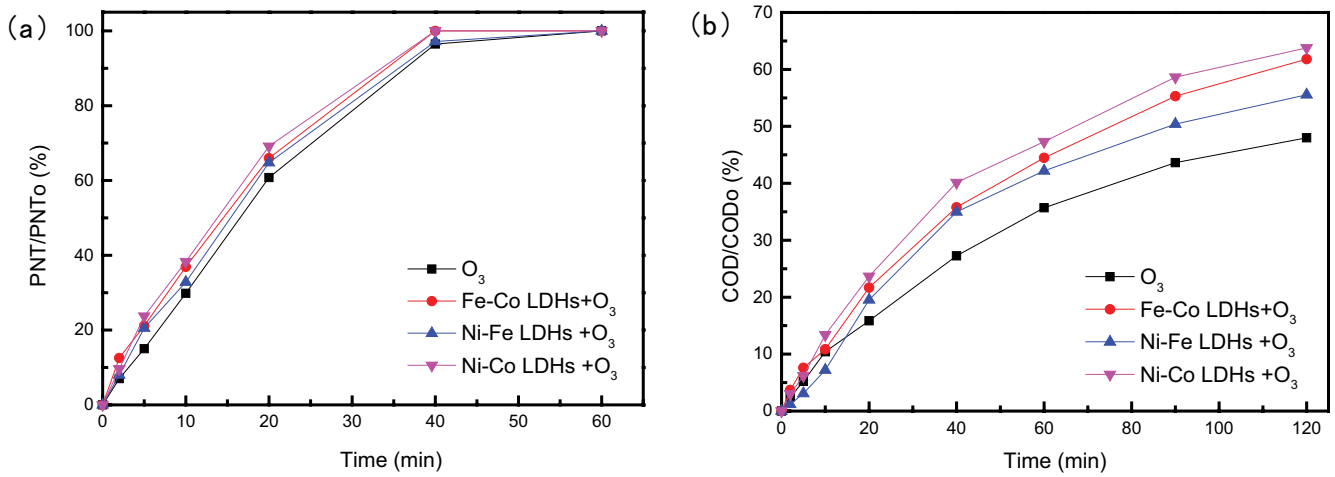

Fig. 4. Catalytic performance of various samples of catalysts: (a) the efficiency of PNT removal and (b) the efficiency of COD removal. Conditions: T = 20°C, $[PNT]_0$ = 200 mg L^{-1}, $[O_3]_0$ = 12 mg L^{-1}, catalyst dosage = 2 g L^{-1}, and pH = 9.0.

within 60 min reaction as shown in Fig. 4a. But significant promotion of COD removal was achieved in synergetic reaction of ozone and the LDHs catalyst (especially Ni–Co LDHs), increasing COD removal of 25%–45% after 20 min reaction in Fig. 4b. The COD removal with Ni–Co LDHs catalyst could reach 63.8%, while 61.8% with Fe–Co LDHs catalyst, 55.5% with Ni–Fe LDHs catalyst and only 48% with ozonation alone after 120 min, indicating that Ni–Co LDHs is an effective catalyst for catalytic ozonation of PNT. The performance of Ni–Co LDHs could be ascribed to the particle surface as characterized by XRD and BET, offered more active sites for PNT decomposition. Ozone molecules are adsorbed on Ni–Co LDH catalyst surface forming weak bonds to hydroxyl groups that cover surfaces of LDH compounds. The Ni–Co ions in 3+ and 4+ oxidation states are very active oxidants. This interaction promotes ozone decomposition, whereas Ni and Co ions mainly acted as active sites for ozone degradation.

Ni–Co LDHs had obvious synergistic effect compared with Ni LDHs and Co LDH with better COD removal rate in120 min. The synergy factor f was detailed to quantify synergy of Ni–Co LDHs, in Eq. (1). The synergistic factors of Ni–Co LDHs were 126% and 116%, respectively, indicating the synergy between cobalt and nickel of Ni–Co LDHs.

$$f = \frac{\eta_{Ni-Co}}{\eta_{Ni/Co}} \times 100\% \quad (1)$$

Among them, η_{Ni-Co}, η_{Ni}, η_{Co} represent the COD removal rate of the PNT in the corresponding process, respectively.

According to the above results, Ni–Co LDHs with better catalytic activity was supported on γ-Al_2O_3 by co-precipitation method to synthesis of Co–Ni LDHs@Al_2O_3 nanoparticles, and the stability tests of catalysts were carried out. Taking experimental deviations into account, three sets of control experiments were performed of pure oxygen with Ni–Co LDHs@Al_2O_3, ozone with Ni–Co LDHs@Al_2O_3, and ozone with Ni–Co LDHs. The metal leaching during the reaction was examined at the same conditions and presented in Table 3. It can be noticed that unstable Ni and Co ions leached from the catalyst to the aqueous solution. The maximum concentration of Ni and Co leached was 2.15 and 2.05 mg L^{-1} on Ni–Co LDHs, the amount of dissolved metal at this level would pose a risk to the aquatic environment since the limit of Ni and Co ions in surface water is 1.0 and 1.0 mg L^{-1} according to the standards in China [38]. The stability of Ni–Co LDHs@Al_2O_3 was investigated under the same experimental conditions, and a significant increase was observed in metal leaching control. It could be inferred from these results that the nanosheets-crosslinked network of Ni–Co LDHs@Al_2O_3 has higher structure stability than the particulate nanosheet-layered structure of Ni–Co LDHs, originating from the interlocking of outstretched nanosheets [39]. Thus, the higher structure stability of Ni–Co LDHs@Al_2O_3 results in its promotion of cycling stability. Therefore, dominant effect of Ni–Co LDHs@Al_2O_3 heterogeneous ozone catalyst is identified in this study.

Table 3
Metal ion leaching in catalytic ozonation of PNT. Conditions: T = 20°C, $[PNT]_0$ = 200 mg L^{-1}, $[O_3]_0$ = 12 mg L^{-1}, catalyst dosage = 2 g L^{-1}, and pH = 9.0

Catalytic ozonation by different catalysts (mg/L)	20 min		60 min		120 min	
	Ni	Co	Ni	Co	Ni	Co
Ni–Co LDHs@Al_2O_3/O_2	0.07	0.05	0.12	0.09	0.17	0.11
Ni–Co LDHs@Al_2O_3/O_3	0.06	0.10	0.21	0.30	0.35	0.40
Ni–Co LDHs/O_3	0.92	1.46	1.74	1.85	2.15	2.05

3.3. Effects of operating parameters

3.3.1. Effect of initial pH value

Solution pH is important because hydroxide ions can initiate ozone self-decomposition which leads to the generation of reactive oxygen species (ROS) [40]. The ozonation of PNT at various initial pH (5, 7, 9, and 11) was examined with an initial concentration of 20°C, 200 mg L^{-1}, ozone

dosage of 12 mg min^{-1} and Ni–Co LDHs@Al_2O_3 dosage of 2 g L^{-1}. As shown in Fig. 5a, the remove rate constants of PNT first increased from 5 to 9 (a maximum) and then decreased with the pH from 9 to 11. This is mainly because increasing solution pH strengthens ozone transformation to $HO_2^{\bullet}$ (the conjugated base of H_2O_2), and enhanced catalytic ozone decomposition by the gradually-deprotonating catalyst [41]. Besides, the electrostatic attraction between the hydrogenated Ni–Co LDHs@Al_2O_3 and the protonated PNT may also make some contribution for the contact of •OH radicals with PNT. However, at pH 11.00, the PNT removal decreased slightly which might due to the excess H_2O_2/$HO_2^{\bullet}$ actually scavenge •OH, thus impeding pollutant degradation and mineralization in Eqs. (2)–(4) [42].

$$^{\bullet}OH + {}^{\bullet}OH \rightarrow H_2O_2 \quad (2)$$

$$^{\bullet}OH + O_3 \rightarrow O_2 + HO_2^{\bullet} \quad (3)$$

$$^{\bullet}OH + HO_2^{\bullet} \rightarrow O_2 + H_2O \quad (4)$$

Apparently, the main contribution of free radicals in the system was the improved elimination of the generated intermediates. In addition, the final pH values after 120 min reaction were also measured and the results showed that pH values of PNT solution dropped rapidly during the reaction. It might be due to the formation of nitrous acid or nitric acid and some organic acids. The decrease in pH might be not conducive to further removal of COD. The catalyst had a certain catalytic effect under the influence of acidic conditions to form metal ions, which had a certain homogeneous catalysis effect. However, it was easy to cause secondary pollution of wastewater, and the homogeneous catalytic effect under acidic conditions was slightly worse than the heterogeneous catalytic effect under basic conditions. It was not conducive to the stability and reuse of the catalyst.

3.3.2. Effect of ozone dosage

The effect of ozone dosage on the removal of PNT and COD during catalytic ozonation was investigated. As shown in Figs. 5c and d, the experiments with 20°C, 200 mg L^{-1} of initial PNT concentration, 2 g L^{-1} of Ni–Co LDHs@Al_2O_3 and pH of 9 were performed using different amounts of ozone, 8, 10, 12, and 14 mg min^{-1}, and the corresponding dissolved ozone concentration were 0.3, 0.5, 0.7, and 0.9 g L^{-1}. The remove rate constants of PNT increased from 60.02% with an O_3 dose of 8 mg min^{-1} to 94.23% with an O_3 dose of 12 mg min^{-1} in 30 min. And the removal of PNT and COD is significantly improved from 8 to 12 mg min^{-1}, but COD removal was not significantly improved from 12 to 14 mg min^{-1}. This ascribed to that the limited active sites on Ni–Co LDHs@Al_2O_3 surface, which would inhibit the further increment of O_3 mass transfer rate from the aqueous phase to the catalyst surface. In addition, the excess O_3 could react with the formed active radicals such as hydroxyl radical, resulting in the decrease of the oxidizing agent for COD removal in Eq. (5). Hence, considering both the real situation of pharmaceutical wastewater and cost-effective analysis, the optimize dosage was chosen as 12 mg min^{-1} in current research.

$$O_3 + 2^{\bullet}OH \rightarrow 2O_2 + H_2O \quad (5)$$

3.3.3. Effect of initial PNT concentration

The effect of initial concentration from 100 to 600 mg L^{-1} was studied at pH 9.0 with ozone dosage of 12 mg min^{-1} and Ni–Co LDHs@Al_2O_3 dosage of 2 g L^{-1}. As shown in Figs. 5e and f, on condition of the initial concentration 100 mg L^{-1}, the PNT reached a quick degradation up to 100% after 20 min of reaction, while for 200, 400, and 600 mg L^{-1}, the results were only 72.80%, 42.38%, and 31.57%, respectively.

It may have two reasons: (1) The removal rate of PNT depends on the number of •OH generated and on the catalytic ability of Ni–Co LDHs@Al_2O_3. Since the higher concentration of PNT, the more oxidizing agent (ozone or free radicals) and active sites were needed. The constant catalyst can only provide limited surface areas and reactive sites, which does not further enhance the reaction between ozone and pollutants as well as the formation of free active radicals. Our experiments were performed under the same operating conditions, so the rate of generation of •OH and the catalytic ability of Ni–Co LDHs@Al_2O_3 were almost constant. Within the limited time, only limited PNT was removed by Ni–Co LDHs@Al_2O_3 process. (2) The more the initial concentration of PNT was the more intermediates generated. And the intermediates generated competed with PNT for •OH. Thus, the apparent reaction constants decreased with an increase of initial concentration.

3.3.4. Effect of catalysts

Replicated experiments and successive runs are important to evaluate the reproducibility of the results and the stability of the catalysts. As shown in Fig. 5g, the experiments of catalysts (Al_2O_3, Ni–Co LDHs, Ni–Co LDHs@Al_2O_3 and repeated experiment) were carried out to evaluate the reproducibility of the results and the stability of the catalysts by the degradation of PNT. The ozonation of PNT was examined with an initial concentration of 20°C, 200 mg L^{-1}, pH 9, ozone dosage of 12 mg min^{-1}, and catalysts dosage of 2 g L^{-1}. After using the catalyst five times, the PNT removal rate was only 3% less than that of the original catalyst after 30 min, and the COD removal rate was reduced by 5% after 60 min of reaction, which indicates that the catalyst can achieve a relatively better reuse effect.

Many literature suggested that surface hydroxyl groups functioned as active sites of solid catalyzer to stimulate the generation of •OH [43]. It was reported that ozone could easily penetrate the LDH structure to approach the transition metals to drive the electron transfer, and this was believed to be a key step in radical chain reactions. Furthermore, the hydroxylated metal ions in LDH acted as Lewis acid sites, which had been verified to be reactive center for catalytic ozonation in aqueous phase [37]. In order to verify whether the catalytic ozonation of PNT belongs to hydroxyl radical reaction mechanism, the experiment was carried out in the

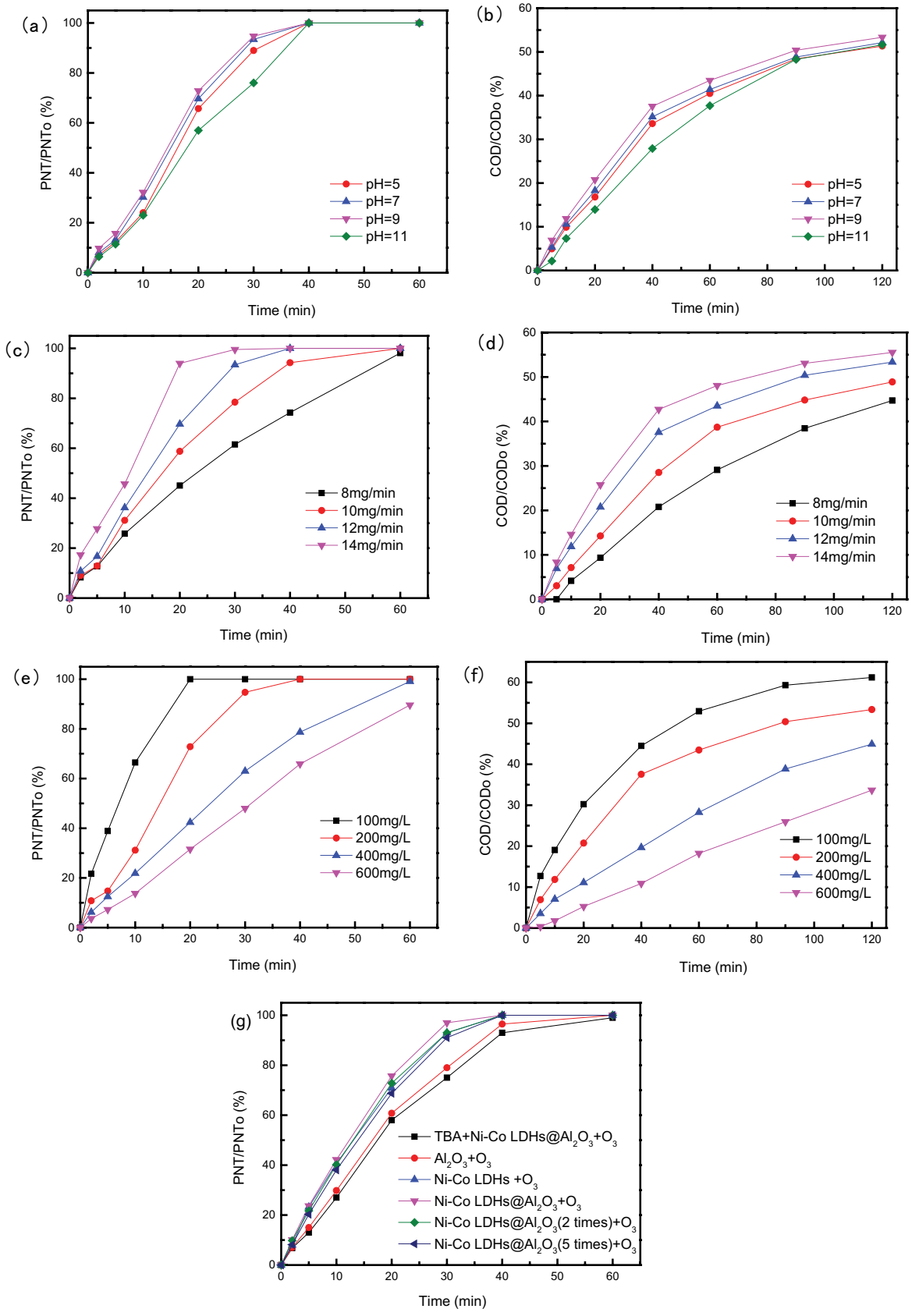

Fig. 5. Variations of PAA and TOC degradation rate: (a and b) effect the initial pH value, (c and d) effect the ozone dosage, (e and f) effect the initial PNT concentration, and (g) effect the catalysts of PNT removal.

presence of *tert*-butyl alcohol (TBA) in Fig. 5g. To clearly investigate the contribution of •OH to the mineralization of PNT during the O_3/Ni–Co LDHs@Al_2O_3 system, and radical quenching experiments were carried out, the presence of 0.1 mol/L TBA remarkably hindered PNT degradation efficiency. After 30 min of reaction, the PNT removal efficiency was 98% in the absence of TBA, but severely reduced to 67% in the presence of TBA. This result revealed that •OH was the main ROS during the O_3/Ni–Co LDHs@Al_2O_3 system. Based on these results, the catalytic mechanism of Ni–Co LDHs@Al_2O_3 could be described briefly. The Ni–Co LDHs@Al_2O_3 catalytic ozonation comprised both surface and bulk reactions. On Ni–Co LDHs@Al_2O_3surface, the generation of free radicals such as •OH was initiated by the electron transfer between different valences of transition metals of Ni and Co. Eqs. (6)–(9) indicated that the decomposition of O_3 occurred and accompanied by the oxidation of M^{2+}, and several reactive species were generated as a result of radical chain reactions.

$$M^{3+} + R \rightarrow M^{2+} + R^{\bullet} \quad (6)$$

$$M^{2+} + O_3 \rightarrow M^{3+} + {}^{\bullet}O_3^- \quad (7)$$

$${}^{\bullet}O_3^- + H^+ \rightarrow HO_3^{\bullet} \quad (8)$$

$$HO_3^{\bullet} \rightarrow O_2 + {}^{\bullet}OH \quad (9)$$

3.4. Probable removal mechanism and degradation pathway

PNT and O_3 molecules may be adsorbed on the catalyst surface. The generation of •OH was confirmed by investigating the effect of •OH inhibitor. Therefore, the presence of PNT could be carried out by an indirect reaction of •OH or direct ozonolytic decomposition. A lot of intermediates were generated during the catalytic ozonation process. Intermediates were detected by GC/MS, IC, and HPLC. On the basis of the intermediates formed in the process of degradation, a probable pathway is proposed and is outlined in Fig. 6. The ozonation reactions can be divided into three reaction type: (1) reaction on the benzene ring, (2) reaction on the amino group, and (3) reaction on the alkyl group. PNT decayed quickly by ozone to generate benzene-ring intermediates that could be degraded later by ozone or •OH depending on the process used. The benzene ring intermediates were divided into five groups: dealkylated, one/two/

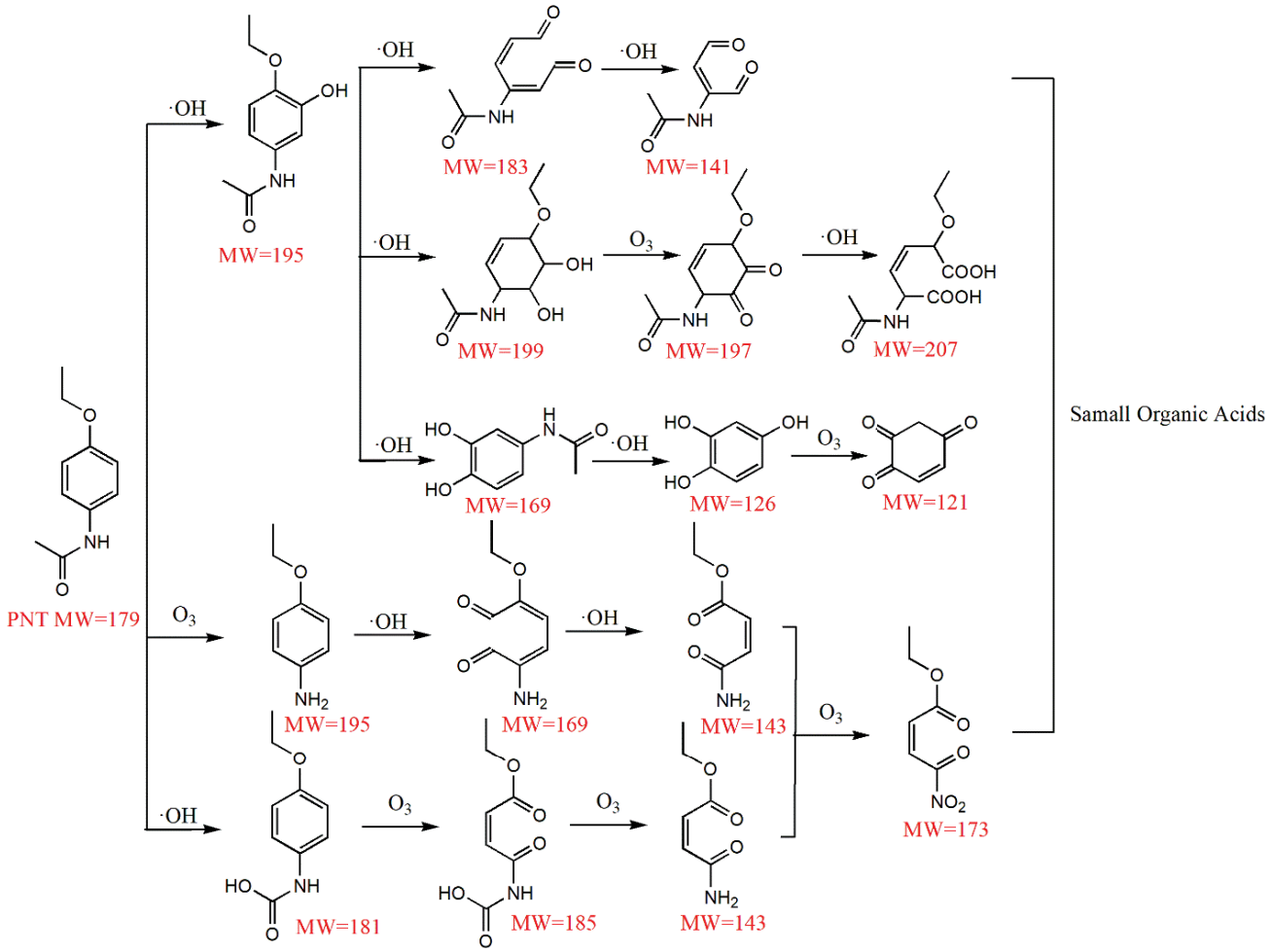

Fig. 6. Proposed degradation pathway of PNT in catalytic ozonation by Ni–Co LDHs@Al_2O_3.

three •OH substituted, and benzene cleavage. Based on the proposed degradation pathway, dealkylated, and two and three •OH substituted intermediates were generated by •OH oxidation, one •OH substituted and benzene cleavage intermediates were formed by both molecular ozone and •OH oxidation. In other pathways, the branched chains of PNT molecule were oxidized firstly with the bond breaking occurs in C–N bond of –NH–C=O. The occurrence of ring-opening reaction via the attack of •OH to the aromatic ring, and it would generate small organic acids. The decrease in the pH value of the solution obtained after ozonation further confirms the presence of organic anions and corresponding acids after PNT degradation.

4. Conclusions

In summary, nanostructured Ni–Co LDHs@Al_2O_3 are prepared by co-precipitation method with continuous nitrogen gas bubbling. The as-prepared Ni–Co LDHs@Al_2O_3 show the 2D nanosheets crosslinked framework with controlled mesopore and strong stability compared with Ni–Co LDHs, and the structure of Ni–Co LDHs@Al_2O_3 catalysts were confirmed by XRD, FT-IR, BET, SEM, and EDX. Ni–Co LDHs@Al_2O_3 which can be separated easily was used as catalyst for catalytic ozonation for the degradation of PNT in aqueous solution, and the degradation mechanisms of PNT were finally discussed. As a result, the presence of Ni–Co LDHs@Al_2O_3 significantly improved both PNT degradation and COD mineralization as compared to ozonation alone. The COD removal with Ni–Co LDHs@Al_2O_3 catalyst could reach 65.3%, while 63.8% with Ni–Co LDHs catalyst, 61.8% with Fe–Co LDHs catalyst, 55.5% with Ni–Fe LDHs catalyst and only 48% with ozonation alone after 120 min. The production of •OH, which played an indispensable role in the destruction of PNT, was greatly promoted by Ni–Co LDHs@Al_2O_3 in the ozonation process. The results may provide further understanding of PNT ozonation mechanisms in water and offer a promising process to treat water contaminated with pharmaceuticals.

Acknowledgments

This research was supported by Zhejiang Provincial Natural Science Foundation of China (LGJ18E080001), National Natural Science Foundation of China (21306175), and the Program for Changjiang Scholars and Innovative Research Team in University (IRT_17R97).

References

[1] M. Rabiet, A. Togola, F. Brissaud, J.L. Seidel, H. Budzinski, F. Elbaz-Poulichet, Consequences of treated water recycling as regards pharmaceuticals and drugs in surface and ground waters of a medium-sized Mediterranean catchment, Environ. Sci. Technol., 40 (2006) 5282–5288.

[2] L. Feng, N. Oturan, E.D. van Hullebusch, G. Esposito, M.A. Oturan, Degradation of anti-inflammatory drug ketoprofen by electro-oxidation: comparison of electro-Fenton and anodic oxidation processes, Environ. Sci. Pollut. Res. Int., 21 (2014) 8406–8416.

[3] F. Qi, W. Chu, B. Xu, Ozonation of phenacetin in associated with a magnetic catalyst $CuFe_2O_4$: the reaction and transformation, Chem. Eng. J., 262 (2015) 552–562.

[4] M. Xiao, Y. Zhang, Electro-catalytic oxidation of phenacetin with a three-dimensional reactor: degradation pathway and removal mechanism, Chemosphere, 152 (2016) 17–22.

[5] O.T. Komesli, M. Muz, M.S. Ak, S. Bakirdere, C.F. Gokcay, Occurrence, fate and removal of endocrine disrupting compounds (EDCs) in Turkish wastewater treatment plants, Chem. Eng. J., 277 (2015) 202–208.

[6] C.G. Daughton, I.S. Ruhoy, Lower-dose prescribing: minimizing "side effects" of pharmaceuticals on society and the environment, Sci. Total Environ., 443 (2013) 324–337.

[7] F. Qi, W. Chu, B. Xu, Comparison of phenacetin degradation in aqueous solutions by catalytic ozonation with $CuFe_2O_4$ and its precursor: surface properties, intermediates and reaction mechanisms, Chem. Eng. J., 284 (2016) 28–36.

[8] Y. Zhu, M. Wu, N. Gao, W. Chu, K. Li, S. Chen, Degradation of phenacetin by the UV/chlorine advanced oxidation process: kinetics, pathways, and toxicity evaluation, Chem. Eng. J., 335 (2018) 520–529.

[9] X.L. Peng, Y.G. Zhang, Y. Liu, Fabrication of a novel high photocatalytic Ag/Ag_3PO_4/P_25 (TiO_2) heterojunction catalyst for reducing electron-hole pair recombination and improving photo-corrosion, Mater. Res. Express, 6 (2019) 065515.

[10] S.J. Wang, C.C. Zhao, D.J. Wang, Y.Q. Wang, F. Liu, (OH)-O-center dot-initiated heterogeneous oxidation of methyl orange using an Fe–Ce/MCM-41 catalyst, RSC Adv., 6 (2016) 18800–18808.

[11] F.J. Real, F.J. Benitez, J.L. Acero, G. Roldan, Combined chemical oxidation and membrane filtration techniques applied to the removal of some selected pharmaceuticals from water systems, J. Environ. Sci. Health., Part A, 47 (2012) 522–533.

[12] S. Khuntia, M.K. Sinha, P. Singh, Theoretical and experimental investigation of the mechanism of the catalytic ozonation process by using a manganese-based catalyst, Environ. Technol., (2019) 1–8, doi: 10.1080/09593330.2019.1640800.

[13] K. El Hassani, D. Kalnina, M. Turks, B.H. Beakou, A. Anouar, Enhanced degradation of an azo dye by catalytic ozonation over Ni-containing layered double hydroxide nanocatalyst, Sep. Purif. Technol., 210 (2019) 764–774.

[14] C.M. Chen, Y. Chen, B.A. Yoza, Y.H. Du, Y.X. Wang, Q.X. Li, L.P. Yi, S.H. Guo, Q.H. Wang, Comparison of efficiencies and mechanisms of catalytic ozonation of recalcitrant petroleum refinery wastewater by Ce, Mg, and Ce–Mg oxides loaded Al_2O_3, Catalysts, 7 (2017) 72.

[15] B. Wang, H. Zhang, F.F. Wang, X.G.Y. Xiong, K. Tian, Y.B. Sun, T.T. Yu, Application of heterogeneous catalytic ozonation for refractory organics in wastewater, Catalysts, 9 (2019) 241.

[16] Y.D. Wang, W.F. Ma, B.A. Yoza, Y.Y. Xu, Q.X. Li, C.M. Chen, Q.H. Wang, Y. Gao, S.H. Guo, Y.L. Zhan, Investigation of catalytic ozonation of recalcitrant organic chemicals in aqueous solution over various ZSM-5 zeolites, Catalysts, 8 (2018) 128.

[17] D. Shahidi, R. Roy, A. Azzouz, Advances in catalytic oxidation of organic pollutants – prospects for thorough mineralization by natural clay catalysts, Appl. Catal., B, 174 (2015) 277–292.

[18] W.L. Wang, H.Y. Hu, X. Liu, H.X. Shi, T.H. Zhou, C. Wang, Z.Y. Huo, Q.Y. Wu, Combination of catalytic ozonation by regenerated granular activated carbon (rGAC) and biological activated carbon in the advanced treatment of textile wastewater for reclamation, Chemosphere, 231 (2019) 369–377.

[19] Y.G. Sun, X. Zhang, N. Li, X. Xing, H.L. Yang, F.L. Zhang, J. Cheng, Z.S. Zhang, Z.P. Hao, Surface properties enhanced Mn_xAlO oxide catalysts derived from Mn_xAl layered double hydroxides for acetone catalytic oxidation at low temperature, Appl. Catal., B, 251 (2019) 295–304.

[20] X.D. Jia, S.J. Gao, T.Y. Liu, D.Q. Li, P.G. Tang, Y.J. Feng, Fabrication and bifunctional electrocatalytic performance of ternary Co/Ni/Mn layered double hydroxides/polypyrrole/reduced graphene oxide composite for oxygen reduction and evolution reactions, Electrochim. Acta, 245 (2017) 51–60.

[21] N.T.K. Phuong, M.W. Beak, B.T. Huy, Y.I. Lee, Adsorption and photodegradation kinetics of herbicide 2,4,5-trichlorophenoxyacetic acid with MgFeTi layered double hydroxides, Chemosphere, 146 (2016) 51–59.

[22] Z. Xu, M. Xie, Y. Ben, J. Shen, F. Qi, Z. Chen, Efficiency and mechanism of atenolol decomposition in Co–FeOOH catalytic ozonation, J. Hazard. Mater., 365 (2019) 146–154.
[23] K.J. Wei, X.X. Cao, W.C. Gu, P. Liang, X. Huang, X.Y. Zhang, Ni-induced C-Al_2O_3-framework ((Ni)CAF) supported core-multishell catalysts for efficient catalytic ozonation: a structure-to-performance study, Environ. Sci. Technol., 53 (2019) 6917–6926.
[24] Y.L. Nie, C. Hu, N.N. Li, L. Yang, J.H. Qu, Inhibition of bromate formation by surface reduction in catalytic ozonation of organic pollutants over β-FeOOH/Al_2O_3, Appl. Catal., B, 147 (2014) 287–292.
[25] O.E. Albertson, Changes in the biochemical oxygen demand procedure in the 21st edition of Standard Methods for the examination of water and wastewater, Water Environ. Res., 79 (2007) 453–455.
[26] A. Alejandre, F. Medina, X. Rodriguez, P. Salagre, Y. Cesteros, J.E. Sueiras, Cu/Ni/Al layered double hydroxides as precursors of catalysts for the wet air oxidation of phenol aqueous solutions, Appl. Catal., B, 30 (2001) 195–207.
[27] R. Danial, S. Sobri, L.C. Abdullah, M.N. Mobarekeh, FTIR, CHNS and XRD analyses define mechanism of glyphosate herbicide removal by electrocoagulation, Chemosphere, 233 (2019) 559–569.
[28] H. Chen, L.F. Hu, M. Chen, Y. Yan, L.M. Wu, Nickel–cobalt layered double hydroxide nanosheets for high-performance supercapacitor electrode materials, Adv. Funct. Mater., 24 (2014) 934–942.
[29] S. Zhao, H.T. Zhu, Z. Wang, P. Song, M. Ban, X.F. Song, A loose hybrid nanofiltration membrane fabricated via chelating-assisted *in-situ* growth of Co/Ni LDHs for dye wastewater treatment, Chem. Eng. J., 353 (2018) 460–471.
[30] R. Elmoubarki, F.Z. Mahjoubi, A. Elhalil, H. Tounsadi, M. Abdennouri, M. Sadiq, S. Qourzal, A. Zouhri, N. Barka, Ni/Fe and Mg/Fe layered double hydroxides and their calcined derivatives: preparation, characterization and application on textile dyes removal, J. Mater. Res. Technol., 6 (2017) 271–283.
[31] Q.Z. Dai, J.Y. Wang, J. Yu, J. Chen, J.M. Chen, Catalytic ozonation for the degradation of acetylsalicylic acid in aqueous solution by magnetic CeO_2 nanometer catalyst particles, Appl. Catal., B, 144 (2014) 686–693.
[32] D.P. Lapham, J.L. Lapham, BET surface area measurement of commercial magnesium stearate by krypton adsorption in preference to nitrogen adsorption, Int. J. Pharm., 568 (2019) 118522.
[33] B.A. Wan, Y.P. Yan, R.X. Huang, D.B. Abdala, F. Liu, Y.Z. Tang, W.F. Tan, X.H. Feng, Formation of Zn–Al layered double hydroxides (LDH) during the interaction of ZnO nanoparticles (NPs) with γ-Al_2O_3, Sci. Total Environ., 650 (2019) 1980–1987.
[34] J. Qu, L. Sha, Z.G. Xu, Z.Y. He, M. Wu, C.J. Wu, Q.W. Zhang, Calcium chloride addition to overcome the barriers for synthesizing new Ca–Ti layered double hydroxide by mechanochemistry, Appl. Clay Sci., 173 (2019) 29–34.
[35] L. Wu, X. Ding, Z.C. Zheng, Y.L. Ma, A. Atrens, X.B. Chen, Z.H. Xie, D.E. Sun, F.S. Pan, Fabrication and characterization of an actively protective Mg–Al LDHs/Al_2O_3 composite coating on magnesium alloy AZ31, Appl. Surf. Sci., 487 (2019) 558–568.
[36] J.P. He, Z.X. Yang, L. Zhang, Y. Li, L.W. Pan, Cu supported on ZnAl-LDHs precursor prepared by *in-situ* synthesis method on γ-Al_2O_3 as catalytic material with high catalytic activity for methanol steam reforming, Int. J. Hydrogen Energy, 42 (2017) 9930–9937.
[37] Y.L. Nie, N.N. Li, C. Hu, Enhanced inhibition of bromate formation in catalytic ozonation of organic pollutants over Fe–Al LDH/Al_2O_3, Sep. Purif. Technol., 151 (2015) 256–261.
[38] L.Y. Qu, H. Huang, F. Xia, Y.Y. Liu, R.A. Dahlgren, M.H. Zhang, K. Mei, Risk analysis of heavy metal concentration in surface waters across the rural-urban interface of the Wen-Rui Tang River, China, Environ. Pollut., 237 (2018) 639–649.
[39] T. Guan, L. Fang, L.L. Liu, F. Wu, Y. Lu, H.J. Luo, J. Hu, B.S. Hu, M. Zhou, Self-supported ultrathin Ni–Co-LDH nanosheet array/Ag nanowire binder-free composite electrode for high-performance supercapacitor, J. Alloys Compd., 799 (2019) 521–528.
[40] W.J. Lee, Y.P. Bao, X. Hu, T.T. Lim, Hybrid catalytic ozonation-membrane filtration process with CeO_x and MnO_x impregnated catalytic ceramic membranes for micropollutants degradation, Chem. Eng. J., 378 (2019) 121670.
[41] P. Gao, Y. Song, S.N. Wang, C. Descorme, S.X. Yang, Fe_2O_3-CeO_2-Bi_2O_3/γ-Al_2O_3 catalyst in the catalytic wet air oxidation (CWAO) of cationic red GTL under mild reaction conditions, Front. Environ. Sci. Eng., 12 (2018) 8.
[42] U. von Gunten, Ozonation of drinking water: part I. Oxidation kinetics and product formation, Water Res., 37 (2003) 1443–1467.
[43] Z.L. Song, Y.T. Zhang, C. Liu, B.B. Xu, F. Qi, D.H. Yuan, S.Y. Pu, Insight into $^{\bullet}OH$ and $^{\bullet}O_2^-$ formation in heterogeneous catalytic ozonation by delocalized electrons and surface oxygen-containing functional groups in layered-structure nanocarbons, Chem. Eng. J., 357 (2019) 655–666.